Journal of Hazardous Materials 433 (2022) 128752

Contents lists available at ScienceDirect

Journal of Hazardous Materials

journal homepage: www.elsevier.com/locate/jhazmat

Research Paper

Uncovering geochemical fractionation of the newly deposited Hg in paddy soil using a stable isotope tracer

Jiang Liu [a], Lei Zhao [b,c,*], Kun Kong [a,d], Mahmoud A. Abdelhafiz [a,d,e], Shanyi Tian [f], Tao Jiang [a,g], Bo Meng [a,**], Xinbin Feng [a]

[a] State Key Laboratory of Environmental Geochemistry, Institute of Geochemistry, Chinese Academy of Sciences, Guiyang 550081, China
[b] School of Management Science, Guizhou University of Finance and Economics, Guiyang 550025, China
[c] Guizhou Key Laboratory of Big Data Statistical Analysis (No. [2019]5103), Guiyang 550025, China
[d] University of Chinese Academy of Sciences, Beijing 100049, China
[e] Geology Department, Faculty of Science, Al-Azhar University, Assiut 71524, Egypt
[f] Soil Ecology Lab, College of Resources and Environmental Sciences, Nanjing Agricultural University, Nanjing 210095, China
[g] Interdisciplinary Research Centre for Agriculture Green Development in Yangtze River Basin, Department of Environmental Sciences and Engineering, College of Resources and Environment, Southwest University, Chongqing 400716, China

HIGHLIGHTS

- Enriched Hg isotope was employed to simulate newly deposited Hg.
- Geochemical fractionation of newly deposited Hg in paddy soil was studied.
- Organic matter is the largest pool of newly deposited Hg in paddy soil.
- Transitions from OM-Hg to Fe/Mn oxide-Hg were observed in paddy soil.
- Coupling of Fe and DOM controlled the fate of newly deposited Hg.

GRAPHICAL ABSTRACT

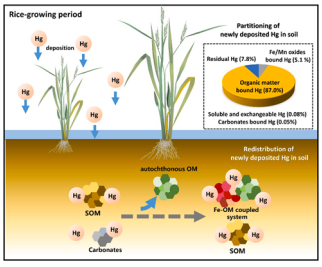

ARTICLE INFO

Editor: Lingxin Chen

Keywords:
Newly deposited Hg
Stable Hg isotope tracer
Geochemical fractionation
Paddy soil

ABSTRACT

The newly deposited mercury (Hg) is more readily methylated to methylmercury (MeHg) than native Hg in paddy soil. However, the biogeochemical processes of the newly deposited Hg in soil are still unknown. Here, a field experimental plot together with a stable Hg isotope tracing technique was used to demonstrate the geochemical fractionation (partitioning and redistribution) of the newly deposited Hg in paddy soils during the rice-growing period. We showed that the majority of Hg tracer (^{200}Hg, 115.09 ± 0.36 μg kg^{-1}) was partitioned as organic matter bound ^{200}Hg (84.6–89.4%), followed by residual ^{200}Hg (7.6–8.1%), Fe/Mn oxides bound ^{200}Hg (2.8–7.2%), soluble and exchangeable ^{200}Hg (0.05–0.2%), and carbonates bound ^{200}Hg (0.04–0.07%) in paddy soils. Correlation analysis and partial least squares path modeling revealed that the coupling of autochthonous dissolved organic matter and poorly crystalline Fe (oxyhydr)oxides played a predominant role in controlling the redistribution of the newly deposited Hg among geochemical fractions (i.e., fraction changes). The expected aging processes of the newly deposited Hg were absent, potentially explaining the high bioavailability of these Hg in paddy soil. This study implies that other Hg pools (e.g., organic matter bound Hg) should be considered instead of merely soluble Hg pools when evaluating the environmental risks of Hg from atmospheric depositions.

* Corresponding author at: School of Management Science, Guizhou University of Finance and Economics, Guiyang 550025, China.
** Corresponding author.
E-mail addresses: zl2047480664@mail.gufe.edu.cn (L. Zhao), mengbo@vip.skleg.cn (B. Meng).

https://doi.org/10.1016/j.jhazmat.2022.128752
Received 23 January 2022; Received in revised form 8 March 2022; Accepted 19 March 2022
Available online 29 March 2022

1. Introduction

Methylmercury (MeHg), the organic form of mercury (Hg), is a broad public concern due to its neurotoxicity, bioaccumulation and biomagnification in food chains. In contrast to other heavy metal pollutants, elemental Hg, the vapor form of Hg could exist in the ambient air, and long-term transportation of this gaseous Hg was widely recoded (Ariya et al., 2015). Consequently, high Hg burdens in biota, especially at high trophic levels, were found in sparsely populated areas (e.g., high latitude lakes) due to the deposition of long-term transported Hg (Lucotte et al., 1999), and the deposition of atmospheric Hg was therefore considered an important Hg source for terrestrial ecosystems.

In recent decades, biogeochemical processes of the newly deposited Hg in terrestrial and aquatic environments have aroused great concerns (Blanchfield et al., 2021; Branfireun et al., 2005; Harris et al., 2007; Hintelmann et al., 2002; Orihel et al., 2008; Oswald et al., 2014; Paterson et al., 2006). A previous study reported that the newly deposited Hg had higher reactivities in reduction and volatilization than native Hg in soils (Hintelmann et al., 2002). Moreover, methylation of the newly deposited Hg was also found to be more active than native Hg in wetland systems (Branfireun et al., 2005) and boreal forest systems (Hintelmann et al., 2002). In a peatland of the Experimental Lakes Area (ELA) in Canada, 6% of newly introduced Hg (used to simulate the newly deposited Hg) was methylated within 24 h (Branfireun et al., 2005). Furthermore, research in aquatic systems documented that the newly deposited Hg is more prone to bioaccumulation in aquatic biota through the formation of MeHg (Harris et al., 2007; Orihel et al., 2008; Paterson et al., 2006).

Rice (*Oryza sativa* L.) is the most important staple food for world populations. In recent studies, however, rice was identified as a bioaccumulator for MeHg (Feng et al., 2011; Meng et al., 2010; Qiu et al., 2008), and health risks for rice-eating people in MeHg exposure were reported (Feng et al., 2008; Zhang et al., 2010). Furthermore, paddy soil, as an ephemeral artificial wetland, was identified as a hotspot of Hg methylation and the major source of MeHg accumulated in rice (Aslam et al., 2022; Liu et al., 2021a; Meng et al., 2010, 2011; Zhao et al., 2016a,b, 2020). Our previous studies confirmed that the newly deposited Hg is more readily methylated to MeHg and accumulates in rice than native Hg in soil (Meng et al., 2010, 2011). The higher bioavailability of the newly deposited Hg in paddy soil was further highlighted in the follow-up studies (Ao et al., 2020; Zhao et al., 2016a). However, the mechanisms behind this finding remain unclear. Therefore, new techniques and more works are urgently needed to uncover the divergent bioavailabilities of native Hg and the newly entered Hg (e.g., newly deposited), especially in Hg-sensitive ecosystems (e.g., rice paddies).

Bioavailability and other factors such as the activity of microorganisms and electron acceptors/donors, resulted in the net production of MeHg (Hsu-Kim et al., 2013) from the newly deposited Hg, which determined the environmental risks of Hg from atmospheric depositions. It is generally accepted that the speciation controls the bioavailability of Hg in biotically mediated methylation (Hsu-Kim et al., 2013; Jonsson et al., 2014; Liu et al., 2022). Typically, Hg speciation in dry or wet depositions is inorganic oxidized Hg (Hg(II)) due to the high deposition velocity (Ariya et al., 2015; Fu et al., 2015) and oxidation events (e.g., atmospheric Hg depletion events, AMDE) in high latitude areas (Schroeder et al., 1998). On the other hand, the speciation changes of the newly deposited Hg in soils are soil chemistry- and particulate-dependent and controlled by the presence of organic matter (Rolfhus et al., 2015), metal (oxyhydr)oxides (O'Connor et al., 2019), sulfur species (Skyllberg, 2008) and clay minerals (Zhu et al., 2012). All of these compounds, in particular, are highly related to the methylation process because they mediate the partitioning and redistribution of Hg among different geochemical fractions (referred to as geochemical fractionation). Therefore, investigating the geochemical fractionation of the newly deposited Hg is critical to understand the behaviors of the newly deposited Hg in methylation as well as corresponding environmental risks.

To fill all the knowledge gaps above, we spiked an isotope-enriched ^{200}Hg tracer to simulate the newly deposited Hg in paddy soils. In addition, the geochemical fractionation processes of spiked ^{200}Hg (i.e., referred to as the newly deposited Hg or "new" Hg) and native Hg (i.e., referred to as ambient Hg or "old" Hg) in paddy soil during the rice-growing period were studied. Furthermore, sequential extractions of Hg (both spiked and native Hg), iron (oxyhydr)oxides and soil organic matter fractions were conducted. The key objectives of this study were to (1) identify the partitioning of "new" Hg in different geochemical fractions in paddy soil, (2) determine the redistribution process of "new" Hg among geochemical fractions during the rice-growing period, and (3) reveal the key factors that potentially control the geochemical fractionation of "new" Hg in paddy soil.

2. Materials and methods

2.1. Study site and rice cultivation experiment

This study was carried out in a regional background area (low Hg concentration in soil and atmosphere), located in Xunyang County, Shannxi Province, China (109°23'24''E, 32°49'48''N). During the rice-growing period, the overall range of gaseous elemental mercury (GEM) at the study site was 1.0–9.0 ng m^{-3} (average 4.8 ± 2.0 ng m^{-3}, Fig. S1). Concentrations of GEM at the study site are slightly higher than the GEM of some remote forest areas (e.g., Mt. Changbai, China, [GEM] = 1.60 ± 0.51 ng m^{-3}, Fu et al., 2012) but lower than those in some urban areas (e.g., Guiyang City, China, [GEM] = 10.2 ± 7.06 ng m^{-3}, Fu et al., 2015) and Hg mining areas (e.g., Wanshan Hg mining area, China, [GEM] = 403 ± 388 ng m^{-3}, Zhao et al., 2016a). Accordingly, low Hg deposition from the atmosphere is expected, which provides ideal conditions when comparing the newly deposited Hg ($^{200}Hg^{2+}$ tracers) and ambient Hg in paddy soil. Therefore, an assumption was made that atmospheric Hg deposition into the experimental plot could be negligible during the rice-growing period.

A simulated rice paddy plot (precleaned polyvinyl chloride box, 54 cm × 42 cm × 33 cm) was set up to investigate the partitioning and redistribution of the newly deposited Hg in paddy soil during the rice-growing period. The soil used in the rice cultivation was collected from cropland (surface soil, 1–20 cm) with a total Hg concentration of 78.4 ± 4.6 μg kg^{-1}. Then, 40 kg pre-sieved soil (2 mm) was filled into the box with a soil depth of approximately 20 cm. Irrigation water (Hg concentration of 1.37 ± 0.45 ng L^{-1}) was added to reach the field moisture capacity. Other physical and chemical properties of the collected soil are shown in Table S1. Isotope-enriched ^{200}Hg ($^{200}Hg(NO_3)_2$), as an inorganic Hg tracer, was spiked into the experimental soil to simulate the newly deposited Hg (Blanchfield et al., 2021; Branfireun et al., 2005; Hintelmann et al., 2002; Oswald et al., 2014). The spiked ^{200}Hg tracer (purity of 98.2 ± 0.15%) was prepared by using $^{200}Hg^0$ (ISOFLEX, USA) according to the methods reported in our previous studies (Liu et al., 2021a, 2022; Meng et al., 2018). Specifically, a working solution of ^{200}Hg tracer (~12 mg Hg L^{-1}, diluted by using deionized water) was prepared to neutral pH and then evenly spiked at ten different positions in the soil of the experimental box. After spiking, the soil in the box was further mixed to homogenize the tracers, and then immediately covered with dark plastic lids (to reduce the potential losses of Hg isotopes) and aged for 24 h before transplanting rice seedlings. The concentration of spiked ^{200}Hg tracer in the studied soil before rice planting is 115.09 ± 0.36 μg kg^{-1}. Notably, oxidized Hg(II), instead of Hg(0), was used as the tracer, as Hg(II) is the dominant species in the atmospheric depositions (Ariya et al., 2015; Fu et al., 2015).

A rice cultivar (hybrid rice), widely grown in Shannxi Province was used in this study. Rice seedlings were pre-cultivated for 30 days. Twenty seedlings with similar biomass and plant height were transplanted to the experimental box with a space of 10 cm × 10 cm. The soil in the box was submerged by irrigation water, and the water level in

each plot was kept at 3–5 cm above the soil surface. Rice in the experimental box was cultivated for 110 days in the field (in an open environment). The water management measures for this study were the same as for local paddy fields (i.e., keep flooding since transplanted and drying from the day 90) to simulate the natural environment for rice-growing. To minimize the perturbation from exogenous chemicals, no fertilizers or pesticides were applied during the rice-growing period. Five sampling campaigns were conducted on the days 0, 30, 60, 90, and 110 after rice transplanting, and 3–5 soil samples from the root zone (10–20 cm depth) were collected into new polypropylene tubes (JET®, China) at each sampling without any headspace. Parafilm® was used to seal the tubes to avoid the potential oxidation during transportation. The collected soil samples were transported to the laboratory within 24 h in coolers with ice packs (~4 °C). Changes of soil physical and chemical properties were minimized. Soil samples were stored at − 20 °C before the freezing dried. The freezing dried (FD-3–85D-MP, FTS, USA) samples were sieved to 200 mesh before measurement. The concentration of GEM close to the experimental box was recorded every 10 s and continuously measured for > 1 h at each sampling in the field.

2.2. Analytical methods

2.2.1. Sequential extraction of Hg

The procedures for sequential extraction of Hg were modified from the method of Tessier et al. (1979). Five fractions were defined as soluble and exchangeable Hg ($Mg(NO_3)_2$ extracted), carbonates bound Hg (NaOAc extracted), Fe/Mn oxides bound Hg ($NH_2OH{\cdot}HCl$ in HAc extracted), organic matter bound Hg (H_2O_2 extracted), and residual Hg (digested by aqua-regia). The details of the extraction procedures are described in Tessier et al. (1979) and were pervasively used by Wang et al. (2011), Zhao (2016), and Li et al. (2019).

2.2.2. Isolation of soil organic matter (SOM) fractions

Soil organic matter was isolated as dissolved organic matter (DOM), humic acid (HA), fulvic acid (FA), clay-associated HA (C-HA), and clay-associated FA (C-FA) (Carter and Gregorich, 2007). DOM was extracted by distilled water (Milli-Q®, Millipore, USA) with a soil-water ratio (*w/v*) of 1:10 (Jiang et al., 2017; Liu et al., 2021b). The details of SOM isolation are shown in Text S1.

2.2.3. Sequential extraction of Fe (oxyhydr)oxides

Iron fractions were extracted as soluble and exchangeable Fe (Fe_{exch}), carbonates associated Fe (Fe_{carb}, siderite, and ankerite), easily reducible Fe oxides (Fe_{ox1}, ferrihydrite, and lepidocrocite), reducible Fe oxides (Fe_{ox2}, goethite, and hematite), magnetite Fe (Fe_{mag}), and pyrite Fe (Fe_{py}) (Text S2). The methods of Fe sequential extraction were established by Poulton and Canfield (2005) and verified by using rock magnetic and X-ray diffraction measurements of pure mineral extractions (Claff et al., 2010; Slotznick et al., 2020).

2.2.4. Measurements

The concentration of GEM was determined by using a portable Hg Vapor Analyzer (RA-915 +, Lumex, Russia). The isotope-enriched $T^{200}Hg$ in soil samples was digested by aqua-regia and determined by using ICP–MS (Agilent 7700 ×, Agilent Technologies Inc., USA) after BrCl oxidation, $SnCl_2$ reduction, and gold trap amalgamation. The method for the isotope-enriched ^{200}Hg after sequential extractions was the same as that for $T^{200}Hg$ after aqua-regia digestion. The isotope-enriched $Me^{200}Hg$ was determined by using gas chromatography (GC)-ICP-MS (Agilent 7700 ×, Agilent Technologies Inc., USA) after ethylation and trapped by Tenax (Brooks, USA) (Gilmour et al., 1998). More details related to the isotope-enriched ^{200}Hg measurements can be found in our previous work (Liu et al., 2021a, 2022). The total amount of organic carbon (TOC) and total nitrogen in soils were measured by an elemental analyzer (Vario MACRO cube, Elementar, Germany) after the removal of inorganic carbon through acidification. Concentrations of each SOM fraction (i.e., DOM, HA, FA, C-HA, C-FA) were determined by a total organic carbon analyzer (InnovOx®, GE, USA). Concentrations of bulk SOM and soil DOM are shown as TOC and DOC, respectively. The optical properties of DOM were characterized by UV–vis absorption and fluorescence spectra through Aqualog® absorption-fluorescence spectroscopy (Jobin Yvon, Horiba, Japan). UV–vis absorption spectra for liquid samples were scanned from 230 nm to 800 nm (1 nm interval). Emission-excitation matrices (EEMs) of fluorescence spectra for liquid samples were scanned from 250 nm to 600 nm for emission spectra and from 230 nm to 450 nm for excitation spectra. Inner-filter effects were corrected according to Wilson and Xenopoulos (2009) and Murphy et al. (2010). Fe in sequential extractions (except pyrite Fe) was reduced by 10% (*w/v*) $NH_2OH{\cdot}HCl$ and quantified by using the ferrozine assay (Viollier et al., 2000). The digestion methods of total Mn and S were the same as those of total Fe. Total Fe, pyrite Fe (nitrate acid extracted in sequential extraction), and total Mn were measured by a flame atomic absorption spectrophotometer (PinAAcle 900 T, PerkinElmer, USA). Total sulfur was measured by a turbidimetric method using a UV–Vis spectrophotometer (UV-5100B, METASH, China) at 420 nm (Sörbo, 1987). Soil pH was determined by a pH meter at a soil-water ratio of 1:2.5 (*w/v*). The X-ray diffraction (XRD) spectra for soil samples were scanned by an X-ray diffractometer (Empyrean, Panalytical, Netherlands) with Cu-K-α radiation from 5° to 60° using 0.025° steps. Soil mineral phases were retrieved by using MDI Jade 6 software (Materials Data Inc., USA).

2.3. Data analysis

Concentrations of ambient THg and MeHg (i.e., Hg that is naturally present in the soil samples) and the isotope-enriched $T^{200}Hg$ and $Me^{200}Hg$ (i.e., ^{200}Hg only from spiked tracer and the ambient ^{200}Hg was deducted) were calculated according to the method detailed in our previous work (Liu et al., 2021a, 2022; Meng et al., 2018). Hg isotope fractionations induced by natural processes were ignored in the isotope-enriched Hg tracer spike studies (Meng et al., 2018). Data analysis for the optical properties of soil DOM is shown in Text S3.

2.4. QA/QC and statistics

Certified reference materials (CRMs) of GSS-5 ([THg] = 290 ± 30 ng g^{-1}) and ERM-CC580 ([MeHg] = 75.5 ± 3.7 ng g^{-1}) were used. The recoveries in THg and MeHg measurements were 109 ± 4.7% (n = 8) and 92 ± 10.0% (n = 10), respectively. The recoveries of mass balance ([the sum of ^{200}Hg fractions] / [$T^{200}Hg$]) for sequential extraction of ^{200}Hg ranged from 86% to 108% (n = 5, Fig. S2). The recoveries of mass balance ([the sum of Hg fractions]/[THg]) for sequential extraction of Hg ranged from 73% to 96% (n = 5). The method detection limits (3σ) were 0.02 μg kg^{-1} for THg, 0.002 μg kg^{-1} for MeHg, and 0.03 μg kg^{-1} for Hg isotopes in soils samples. The relative standard deviation (RSD) for duplicates was less than 10%.

The differences in data sets that were normally distributed were assessed by t–test and one-way ANOVA with Duncan's post-hoc test using SPSS 23.0 (IBM®, IL, USA). The differences tests for nonnormally distributed datasets were accessed by Kruskal–Wallis one-way ANOVA. The statistical significance (p) was declared at < 0.05 (2-tailed). The partial least squares path modeling (PLS-PM) was conducted by using R software (version 4.1.2) that was equipped with the "plspm" package.

3. Results

3.1. The isotope-enriched ^{200}Hg and ambient Hg

Concentrations of the isotope-enriched $T^{200}Hg$ and ambient THg in paddy soil during the rice-growing period were stable, with various ranges of 104.04 ± 2.91–120.65 ± 8.56 ng g^{-1} and 73.07 ± 4.29–95.04 ± 17.12 ng g^{-1}, respectively (Fig. S3a). It is worth mentioning that the

concentrations of spiked $T^{200}Hg$ and ambient THg are comparable, indicating that the spiked isotope tracers in this study can reflect the practical situation of Hg fate in paddy soil (Branfireun et al., 2005; Hintelmann et al., 2002; Oswald et al., 2014).

Since the spiking of Hg isotope tracers into paddy soil, most parts of the spiked ^{200}Hg were partitioned into organic matter bound Hg (84.6–89.4% of $T^{200}Hg$), followed by residual ^{200}Hg (7.6–8.1% of $T^{200}Hg$), and then Fe/Mn oxides bound ^{200}Hg (2.8–7.2% of $T^{200}Hg$) (Kruskal–Wallis one-way ANOVA $p < 0.01$, Figs. 1a and b). Soluble and exchangeable ^{200}Hg (0.05–0.17% of $T^{200}Hg$) and carbonates bound ^{200}Hg (0.04–0.07% of $T^{200}Hg$) governed only a small proportion of $T^{200}Hg$ (Figs. 1a and b). A similar distribution pattern was found in the ambient Hg fractions (i.e., organic matter bound Hg > residual Hg > Fe/Mn oxides bound Hg > exchangeable Hg > carbonates bound Hg). Nevertheless, relatively higher residual Hg (23.9–37.9% of THg, Kruskal–Wallis one-way ANOVA $p < 0.01$) but lower Fe/Mn oxides bound Hg (2.4–6.2% of THg, paired samples t-test $p < 0.05$) and organic matter bound Hg (57.4–73.5% of THg, paired samples t-test $p < 0.01$) were observed for ambient Hg than those of spiked ^{200}Hg (Figs. 1c and d, Fig. S4).

During the rice-growing period, the decreases in soluble and exchangeable Hg (both ^{200}Hg and ambient Hg) ^{200}Hg, carbonates bound ^{200}Hg, organic matter bound Hg (both ^{200}Hg and ambient Hg), and residual ^{200}Hg were observed (one-way ANOVA $p < 0.05$, Figs. 1a and c, Figs. S5 and S6). The significant increases in Fe/Mn oxides bound ^{200}Hg were found from the day 30–60 (from 3.30 ± 0.24 ng g^{-1} to 6.01 ± 1.13 ng g^{-1}, one-way ANOVA $p < 0.05$, Fig. 1a and Fig. S5). The variations in $Me^{200}Hg$ and ambient MeHg during the rice-growing period are shown in the Fig. S3b and Text S4.

3.2. Soil organic matters and optical properties of soil DOM

Different soil organic matter fractions play key roles in regulating the fate of Hg (Xu et al., 2021). Moreover, organic matter bound Hg was identified as the largest pool for the newly deposited Hg in paddy soil (Fig. 1); therefore, soil organic matter fractions were investigated. As shown in Fig. 2, the decreases in total organic carbon (TOC, showing the concentration of bulk SOM) but increases in dissolved organic carbon (DOC, showing the concentration of soil DOM) in paddy soils were observed during the rice-growing period (one-way ANOVA $p < 0.05$). Soil humic substances were isolated as humic acid (HA), fulvic acid (FA), and clay-associated HA and FA. In detail, the significant increases in HA and FA were found from the day 60 to day 110 in paddy soil (Fig. 2b, one-way ANOVA $p < 0.05$), whereas the HA and FA associated with soil clays decreased (Fig. 2c, a significant difference was only found in C-HA, one-way ANOVA $p < 0.05$).

Both UV–vis absorption and fluorescence spectra were used to calculate the optical properties of soil DOM. Through UV–vis absorption

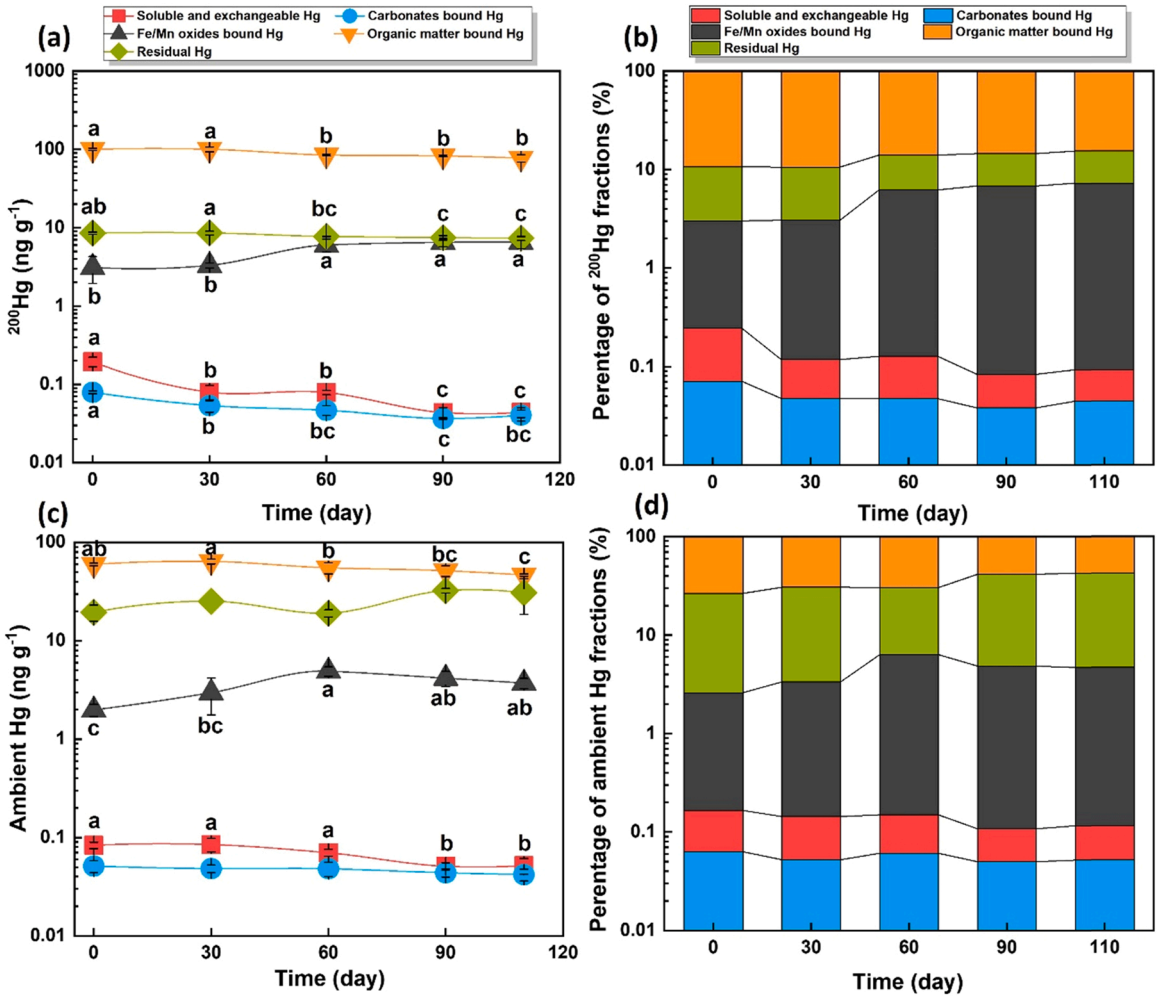

Fig. 1. Concentration and percentage of isotope-enriched ^{200}Hg (a and b) and ambient Hg (c and d) fractions in paddy soils during the rice-growing period. Different lowercase letters in line plots indicate that the differences in Hg concentration in paddy soils during the rice-growing period are significant through one-way ANOVA with Duncan's post-hoc test ($p < 0.05$). Data without lowercase letters suggest the difference is not significant. Error bars in line plots represent the standard deviation of three replicates (five replicates on day 110). All the units were presented by dry weight.

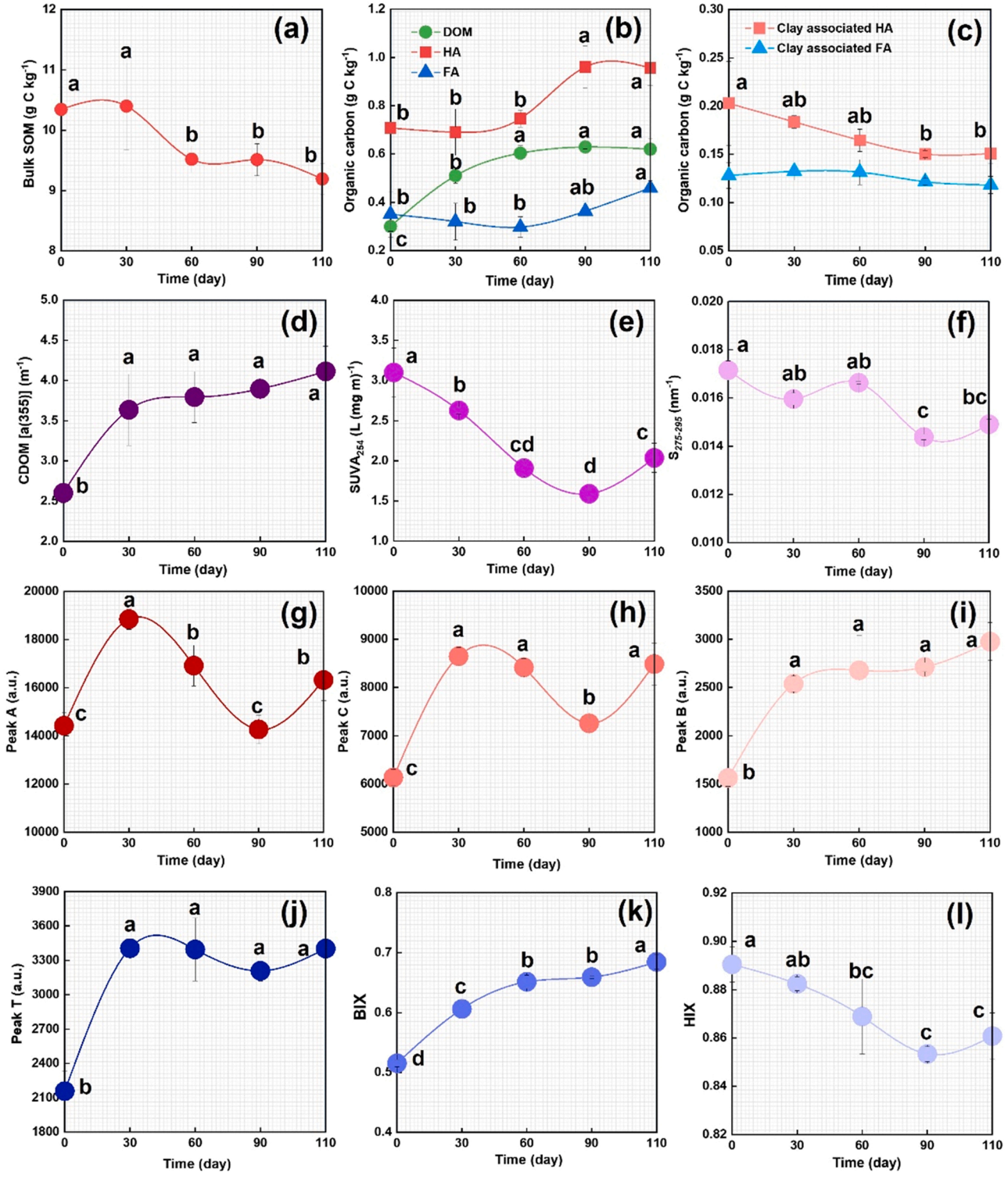

Fig. 2. Concentrations of bulk soil organic matter (SOM) (a), dissolved organic matter (DOM), humic acid (HA), fulvic acid (FA) (b), clay-associated HA and FA (c) and the optical properties of DOM (d-l) in paddy soils during the rice-growing period. Plots (d) to (f) are the properties from UV–vis absorption spectra of DOM, including the absorption coefficient at 355 nm (used to represent colored dissolved organic matter, $a(355)$) (d), specific UV absorbance at a wavelength of 254 nm ($SUVA_{254}$) (e), and spectral slope of 275–295 nm ($S_{275-295}$) (f). Plots (g) to (l) are the fluorescence compounds and calculated indices from EEM fluorescence spectra of DOC, including peak A (g), peak C (h), peak B (i), peak T (j), biological index (BIX) (k), and humification index (HIX) (l). Different lowercase letters indicate that the difference is significant through one-way ANOVA with Duncan's post-hoc test ($p < 0.05$). Data without lowercase letters suggest the difference is not significant. The error bar represents the standard deviation of three replicates (five replicates on day 110). All the units of mass were presented by dry weight.

spectra, increased signals of CDOM were found during the rice-growing period (Fig. 2d, one-way ANOVA $p < 0.05$), whereas the decreases in $SUVA_{254}$ (Fig. 2e, from the day 0 to day 90, one-way ANOVA $p < 0.05$) and $S_{275–295}$ (Fig. 2f, from the day 60 to day 90, one-way ANOVA $p < 0.05$) were observed. $SUVA_{254}$ increased after the decline from the first 90 days. Fluctuations of the intensities of fulvic-like (i.e., peak A, less humified) and humic-like compounds (i.e., peak C, more humified) and higher intensities of peak A than that of peak C were obtained (Figs. 2 g and h, one-way ANOVA $p < 0.05$). With the growth of rice, more signals of protein-like (or fresh-like) compounds (Figs. 2i and j, one-way ANOVA $p < 0.05$) and higher autotrophic productivity (shown as BIX, Fig. 2k, one-way ANOVA $p < 0.05$) values were found in soil DOM. Nevertheless, the humification degree, shown as HIX, decreased during the rice-growing period (Fig. 2l, one-way ANOVA $p < 0.05$).

3.3. Total Fe, Mn, and Fe fractions

In addition to organic matter bound Hg, Fe/Mn oxides bound Hg was also an important pool for the newly deposited Hg in paddy soil (Fig. 1). Typically, Fe and Mn coexist in soils such as ferromanganese nodules (Liu, C. et al., 2021c; Tessier et al., 1979), and the environmental behaviors of Fe and Mn oxides are quite similar. In this study, the concentration of total Fe (TFe, averaged 31.2 ± 0.8 g kg^{-1}) was more than 70 times higher than that of total Mn (TMn, averaged 0.42 ± 0.01 g kg^{-1}) during the rice-growing period (Fig. S7). Therefore, Fe fractions (i.e., Fe (oxyhydr)oxides) were further extracted to show the influences of Fe/Mn oxides on the fate of "new" Hg. During the rice-growing period, the percentage of highly reactive Fe (Fe_{HR}) in TFe in rice paddy soil was stable, and no significant variation was observed (Table 1). The largest Fe pool in Fe_{HR} is reducible Fe oxides (Fe_{ox2}, crystalline Fe oxides), followed by magnetite Fe, easily reducible Fe oxides, pyrite Fe, and carbonate-bound Fe. The significant increases in Fe_{carb} (one-way ANOVA $p < 0.05$), Fe_{ox1} (one-way ANOVA $p < 0.05$), and Fe_{py} (one-way ANOVA $p < 0.05$) were found in paddy soil during the rice-growing period (Table 1). Magnetite Fe decreased from the day 30 to the end of the experiment (one-way ANOVA $p < 0.05$), and Fe_{ox2} decreased during the whole rice-growing period (one-way ANOVA $p < 0.05$) (Table 1). Due to the relatively stable Fe_{HR} concentration and Fe_{HR}/TFe, the increases in Fe_{carb}, Fe_{ox1}, and Fe_{py} were offset by the decreases in Fe_{ox2} and Fe_{mag} (one-way ANOVA $p < 0.05$). No crystalline structures of Fe(oxyhydr)oxides were identified through XRD (Fig. S8), which may be attributed to the poor crystalline structures or the formation of micro/nanometric Fe(oxyhydr)oxides under redox conditions (Bishop et al., 2020; Ratié et al., 2019). More descriptions of ancillary data (soil pH, total sulfur, total nitrogen, and the C/N ratio) are shown in the Text S5 in the Supporting Information.

3.4. Relationships between the isotope-enriched ^{200}Hg and geochemical factors

Through the correlation analysis, all the isotope-enriched ^{200}Hg fractions (i.e., soluble and exchangeable ^{200}Hg, carbonates bound ^{200}Hg, Fe/Mn oxides bound ^{200}Hg, organic matter bound ^{200}Hg, and residual ^{200}Hg fractions) were significantly correlated with DOM, $a(355)$, BIX, HIX, Fe_{carb}, Fe_{ox1}, and Fe_{ox2} (Table 2). For example, Fe/Mn oxides bound to ^{200}Hg are highly co-varied with soil humic acid (Spearman's $r = 0.77$, $p < 0.01$, $r^2 = 0.51$), DOM (Spearman's $r = 0.91$, $p < 0.01$, $r^2 = 0.72$), protein-like fluorescence compounds (i.e., peak B, Spearman's $r = 0.76$, $p < 0.01$, $r^2 = 0.39$) and BIX (Spearman's $r = 0.67$, $p < 0.01$, $r^2 = 0.55$) (Fig. 3 and Table 2). It is noted that soil DOM is negatively correlated with soluble and exchangeable ^{200}Hg, carbonates bound ^{200}Hg, organic matter bound ^{200}Hg, and residual ^{200}Hg, but positively correlated with Fe/Mn oxides bound ^{200}Hg (Fig. 3). Similar tendency of correlations was also found in BIX and Fe_{ox1}.

Four latent variables, including soil chemistry (including total sulfur, total Fe, total Mn, total N, pH, and C/N ratio), soil bulk OM (including TOC, humic acid, fulvic acid, and clay-associated humic acid and fulvic acid), DOM (including DOC, $SUVA_{254}$, $S_{275–295}$, peak A, peak B, BIX, and HIX), and Fe species (including Fe_{exch}, Fe_{carb}, Fe_{ox1}, Fe_{ox2}, and Fe_{mag}), were input for partial least squares path modeling analysis. The goodness-of-fit (GOF) ranged from 0.57 to 0.60, showing a good model predictive value (Fig. 4). Through Fig. 4, DOM (path coefficient of −0.42) and Fe (oxyhydr)oxides (path coefficient of −0.39) are two major effects for soluble and exchangeable ^{200}Hg, whereas DOM (path coefficient of −0.50) is the major effect for carbonates bound ^{200}Hg (Figs. 4a and b). For Fe/Mn oxides bound ^{200}Hg, DOM showed the most considerable effect (path coefficient of 0.86, Fig. 4c). In addition to bulk SOM and DOM, Fe species also showed a high contribution (path coefficient of −0.43) to organic matter bound ^{200}Hg (Fig. 4d).

4. Discussions

4.1. Partitioning of "new" Hg in different geochemical fractions in paddy soil

Through sequential extraction, organic matter was identified as the largest sink of both newly spiked and ambient Hg in paddy soil (Fig. 1). This finding is consistent with our previous works in paddy soil at an artisanal Hg smelting site (i.e., Wanshan Hg mining area, [THg] = 3.2 ± 0.75 mg kg^{-1}, organic matter bound Hg could reach 62% of THg, Zhao, 2016) and in the background soil of urban areas (i.e., Huaxi, Guiyang City, [THg] = 0.25 ± 0.06 mg kg^{-1}, organic matter bound Hg could reach 87.8% of THg, Lu et al., 2021). These results highlighted that organic matter could be the largest pool for the Hg from atmosphere depositions. Soil organic matter is regarded as one of the most important Hg sinks due to (1) its high binding affinity with Hg and (2) its association with Hg-adsorbing particles (O'Connor et al., 2019). In particular, the majority of "new" Hg in the soil is partitioned into the solid phase (e.g., soil minerals) since deposition, and only a small fraction of the newly deposited Hg in the soil is present in the aqueous phase (e.g., porewater) (Jonsson et al., 2014). Furthermore, research has documented that soil minerals are often coated with organic matter (Lalonde et al., 2012; Riedel et al., 2013), and the adsorption behaviors of soil minerals for Hg are profoundly influenced by this organic matter (Zhang et al., 2019),

Table 1
Concentration of total Fe and various Fe pools in paddy soils during the rice-growing period.

Rice-growing period	TFe	Fe_{exch}	Fe_{carb}	Fe_{ox1}	Fe_{ox2}	Fe_{mag}	Fe_{py}	Fe_{HR}	Fe_{HR}/TFe
(day)	(g kg^{-1})	(mg kg^{-1})	(g kg^{-1})	(g kg^{-1})	(g kg^{-1})	(g kg^{-1})	(g kg^{-1})	(g kg^{-1})	(%)
0	32.1 ± 2.2	1.29 ± 0.5	0.005 ± 0.0004c	0.37 ± 0.03d	8.43 ± 0.3a	1.77 ± 0.1ab	0.59 ± 0.03b	11.2 ± 0.2ab	34.8 ± 1.8
30	31.3 ± 0.9	1.20 ± 0.2	0.067 ± 0.01c	0.87 ± 0.05c	7.34 ± 0.4b	1.95 ± 0.3a	0.60 ± 0.04b	10.8 ± 0.2b	35.5 ± 0.9
60	30.0 ± 0.5	1.31 ± 0.2	0.23 ± 0.02b	1.19 ± 0.06b	7.13 ± 0.4 bc	1.84 ± 0.09ab	0.75 ± 0.1ab	11.1 ± 0.3ab	36.3 ± 1.4
90	30.8 ± 1.0	1.37 ± 0.2	0.45 ± 0.04a	1.42 ± 0.01a	7.01 ± 0.03 bc	1.65 ± 0.02b	0.70 ± 0.09ab	11.2 ± 0.05a	36.8 ± 0.3
110	31.7 ± 1.4	1.28 ± 0.5	0.49 ± 0.10a	1.45 ± 0.05a	6.56 ± 0.4c	1.66 ± 0.1b	0.87 ± 0.2a	11.0 ± 0.2ab	34.5 ± 1.0

TFe is total Fe; Fe_{exch} is soluble and exchangeable Fe; Fe_{carb} is carbonates bound Fe; Fe_{ox1} is easily reducible Fe; Fe_{ox2} is reducible Fe; Fe_{mag} is magnetite Fe; Fe_{py} is pyrite Fe; Fe_{HR} is highly reactive Fe ($FeHR = \sum (Fe_{exch} + Fe_{carb} + Fe_{ox1} + Fe_{ox2} + Fe_{mag} + Fe_{py})$). Different lowercase letters in each column indicate that the differences in Fe concentrations in paddy soils at different rice-growing periods are significant through one-way ANOVA with Duncan's post-hoc test ($p < 0.05$). All the units of mass were presented by dry weight

Table 2
Correlation matrix between ^{200}Hg fractions and geochemical factors.

	Soluble and exchangeable ^{200}Hg	Carbonates bound ^{200}Hg	Fe/Mn oxides bound ^{200}Hg	Organic matter bound ^{200}Hg	Residual ^{200}Hg
TS	0.85**	0.80**		0.73**	0.55*
TFe					
TMn					
pH					
TOC				0.48*	
C/N					
HA	-0.85**		0.77**	-0.68**	-0.56*
FA	-0.58*				
C-HA	0.87**	0.84**		0.82**	0.72**
C-FA					
DOC	-0.67**	-0.55*	0.91**	-0.68**	-0.074**
a(355)	-0.73**	-0.57*	0.67*	-0.77**	-0.65*
$SUVA_{254}$	0.58*	0.58*	-0.87**		0.65*
$S_{275–295}$	0.70**		-0.79**	0.57*	0.52*
peak A					
peak B	-0.66*		0.76**	-0.71**	-0.60*
peak C					
peak T					
BIX	-0.86**	-0.65**	0.67**	-0.82**	-0.72**
HIX	0.76**	0.66**	-0.79**	0.61**	0.65**
Fe_{exch}					
Fe_{carb}	-0.94**	-0.66**	0.79**	-0.74**	-0.68**
Fe_{ox1}	-0.91**	-0.62**	0.79**	-0.74**	-0.71**
Fe_{ox2}	0.76**	0.68**	-0.61**	0.65**	0.68**
Fe_{mag}	0.58*			0.54*	
Fe_{py}	-0.52*		0.65**	-0.62**	-0.72**

Spearman's r was used as the correlation coefficient. "*" and "**" indicate that the correlations are significant at $p < 0.05$ and $p < 0.01$. Vacancies suggest that the correlations are not significant. Abbreviations: TS, total sulfur; TFe, total iron; TMn, total manganese, TOC, total organic carbon; C/N, carbon and nitrogen ratio; HA, humic acid; FA, fulvic acid; C-HA, clay-associated HA; C-FA, clay-associated FA; DOC, dissolved organic carbon; a(355), absorption coefficient at 355 nm; $SUVA_{254}$, specific UV absorbance at a wavelength of 254 nm; $S_{275–295}$, spectral slope of 275–295 nm; peaks A, B, C, and T, fluorescence compounds; BIX, biological index; HIX, humification index; Fe_{exch}, soluble and exchangeable Fe; Fe_{carb}, carbonate associated Fe; Fe_{ox1}, easily reducible Fe oxides; Fe_{ox2}, reducible Fe oxides; Fe_{mag}, magnetite Fe; Fe_{py}, pyrite Fe.

such as thiol ligands (-RSH) associated with the organic matter (Skyllberg et al., 2006; Skyllberg, 2008) under reduced conditions. As a result, the retention of "new" Hg by organo-minerals (i.e., organic matter-coated minerals) is an important reason that explains the high partitioning of the newly deposited Hg in organic matter. In addition, the formation and stabilization of nanoparticulate or colloidal HgS originating from "new" Hg are highly influenced by organic matter (Gerbig et al., 2011; Graham et al., 2012), and this Hg pool is commonly found in anoxic environments (e.g., paddy soil) and cannot be ignored (Manceau et al., 2018).

Traditionally, sulfides are the major sink of Hg in natural environments, especially in Hg mining areas (Yin et al., 2016). However, due to the lower amount of total sulfur than SOM (Fig. 2 a and Fig. S9) and the redox fluctuation (i.e., dry-wet alterations in paddy soils), the pool size of residual ^{200}Hg (typically HgS) only accounts for 7.6–8.1% of the T^{200}Hg pool. The unexpectedly low partitioning of "new" Hg into residual Hg suggests that the kinetics of Hg-soil organic matter binding are faster than the formation of HgS particles, which is consistent with previous studies showing that organic matter is the rate-limited factor for the aggregation of HgS clusters (Gerbig et al., 2011; Graham et al., 2012; Hsu-kim et al., 2013). Well-structured mineral lattices are also Hg sinks (forming residual Hg pools, Tessier et al., 1979); however, the entrance or replacement of Hg into those lattices (e.g., silicate lattices) is usually slower than binding with organic matter. This also supports the low partitioning of "new" Hg into residual Hg.

Metal oxides are also one of the sinks for trace metals in soil, and numerous studies have reported high adsorption capacities of Fe/Mn oxides for Hg (Bonnissel-Gissinger et al., 1999; Feyte et al., 2010). This explained that Fe/Mn oxides are the third pool of "new" Hg only to organic matter bound Hg and residual Hg (Fig. 1). However, this Hg pool varied with the oxide phase changes driven by redox alternations, which was supported by variations in Hg distribution (Fig. 1) and Fe(oxyhydr) oxide changes during the rice-growing period (Table 1).

The spiked ^{200}Hg into paddy soil is dissolved $^{200}Hg(NO_3)_2$; therefore, a large fraction of soluble and exchangeable Hg was excepted. However, the partitioning of "new" Hg into soluble and exchangeable Hg and carbonates bound Hg only accounts for a minor fraction (0.09–0.24%) of T^{200}Hg, suggesting that the strong binding sites (e.g., surface complexation sites, adsorption sites) for Hg are far from saturated in paddy soil and the newly deposited Hg will be immobilized immediately.

4.2. *Redistribution of "new" Hg among different geochemical fractions during the rice-growing period*

The redistribution of the newly deposited Hg among geochemical pools can be revealed by variations in different ^{200}Hg pools during the rice-growing period (Fig. 1a). In this study, transitions from soluble and exchangeable ^{200}Hg, carbonates bound ^{200}Hg, organic matter bound ^{200}Hg, and residual ^{200}Hg to Fe/Mn oxides bound ^{200}Hg were found (Fig. 3a). Redistribution of soluble and exchangeable ^{200}Hg and carbonates bound ^{200}Hg occurred initially after spiking with ^{200}Hg tracers, suggesting an immobilization process of these highly liable Hg pools. However, transitions of organic matter bound ^{200}Hg, Fe/Mn oxides bound ^{200}Hg and residual ^{200}Hg mainly occurred after 30 days. This suggests that although "new" Hg rapidly partitioned into the solid phase after deposition, the redistribution among these three Hg pools (i.e., Fe/Mn oxides bound Hg, organic matter bound Hg and residual Hg) took time to reach equilibrium. Two reasons may be explained for the redistribution of "new" Hg in environments: one is the thermodynamic equilibrium process of Hg in soil, and the other is the biogeochemical condition change-induced re-equilibrium process. The former is likely responsible for the decreases in soluble and exchangeable ^{200}Hg and carbonates bound ^{200}Hg because dissolved phases (e.g., soluble Hg) are not stable in the presence of colloids or solids (Skyllberg et al., 2021), which will be redistributed into colloids or solids rapidly. Nevertheless, the latter (i.e., re-equilibrium process) may play a dominant role in the redistribution of "new" Hg among geochemical pools due to the highly dynamic biogeochemistry of paddy soil (Kögel-Knabner et al., 2010).

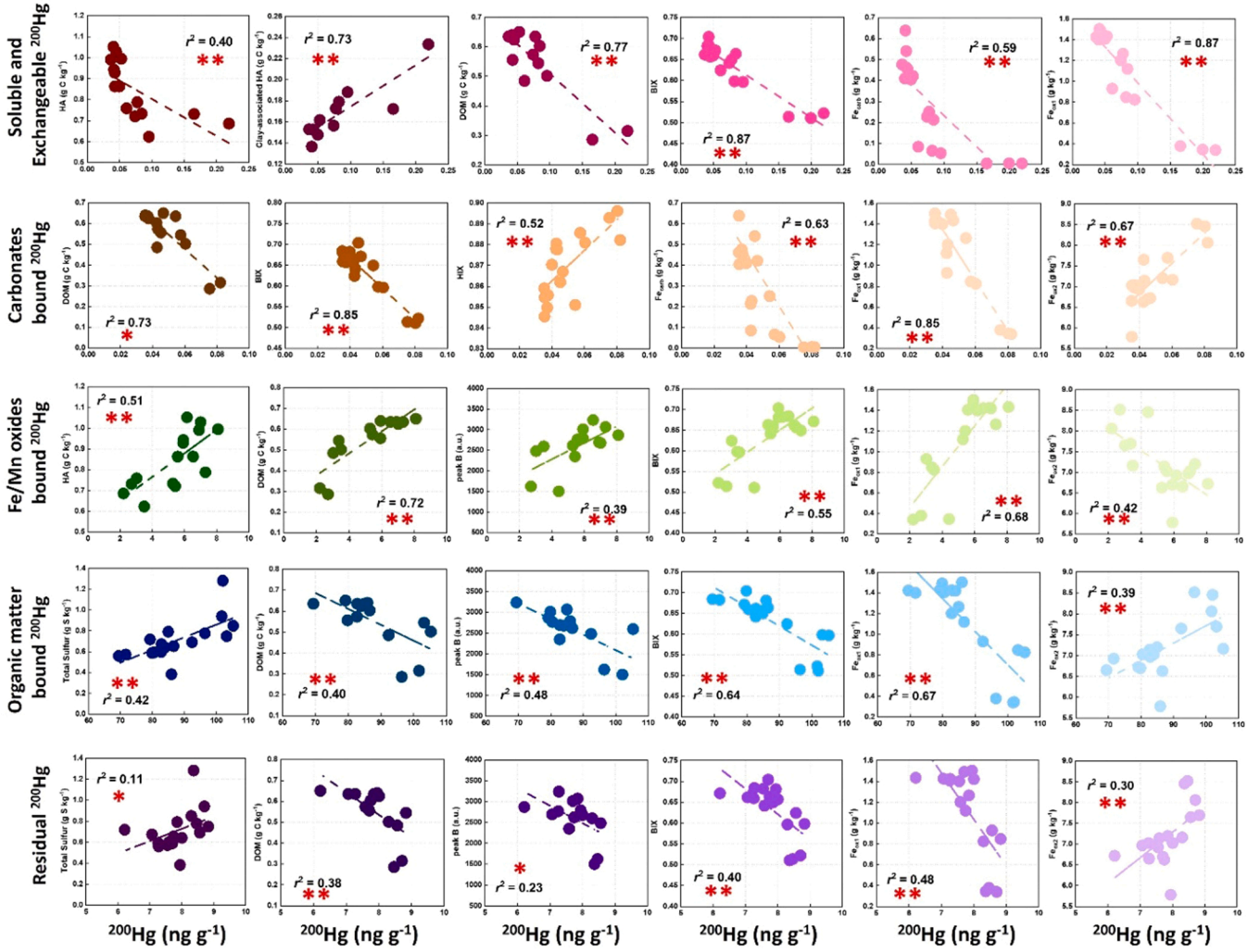

Fig. 3. Concentration of isotope enriched ^{200}Hg in different fractions versus various geochemical factors. r^2 is the determination coefficient from linear regression, "* " and "* *" suggest that the correlation between two variables is significant at $p < 0.05$ and $p < 0.01$. Abbreviations: HA is humic acid, DOM is dissolved organic matter, BIX is biological index, HIX is humification index, peak B is a fluorescence compound with protein-like character, Fe_{carb} is carbonate-associated Fe, Fe_{ox1} is easily reducible Fe oxides, and Fe_{ox2} is reducible Fe oxides. All the units of mass were presented by dry weight.

For example, changes in both the concentration and structural composition of soil organic matter (Fig. 2) coupled with the decreases in organic matter bound ^{200}Hg (Fig. 1a) indicate the release of "new" Hg from OM in paddy soil during the rice-growing period. Specifically, mineralization of SOM and production of dissolved OM fractions in this study were evidenced by the decreased TOC (Fig. 2a) and increased water-soluble organic carbon (Fig. 2b) during the rice-growing period. Moreover, significant negative correlations between organic matter bound to ^{200}Hg and the concentration of DOM (Spearman's $r = -0.68$, $p < 0.01$) and autochthonous signals of DOM (Peak B, Spearman's $r = -0.71, p < 0.01$; BIX, Spearman's $r = -0.82, p < 0.01$) can be found in Fig. 3. These findings demonstrate that mineralization of SOM and production of dissolved OM through microbial metabolism (Liu et al., 2021b), especially in the rhizosphere, could release "new" Hg from SOM. A similar result was reported in permafrost areas, in which OM decomposition induced by permafrost degradation posed a great risk to Hg release (Mu et al., 2020). Furthermore, the secretion of root exudates in the rhizosphere may have a priming effect on the mineralization of SOM in paddy soil (Du et al., 2020), which may also promote the release of Hg from SOM. It is noted that this study is not to discuss the absorption, translocation and bioaccumulation of Hg tracers in soil-rice systems. Therefore, the data for the isotope-enriched ^{200}Hg, and ambient Hg in rice tissues were not studied. However, translocation and transformation of Hg in rice plants were reported in a parallel work with similar experimental design but conducted at a different site (high GEM region) (Liu et al., 2021a).

An interesting finding of this study is that Fe/Mn oxides are sinks for the newly deposited Hg in redistribution. Due to the coexistence and similar environmental behaviors of Fe and Mn oxides (Liu, C. et al., 2021c; Tessier et al., 1979), as well as higher concentrations of total Fe than Mn in soils (Fig. S7). This study takes Fe oxides as an example to show the influence of Fe/Mn oxides on "new" Hg. Significant enrichment of ^{200}Hg was found in poorly crystalline or amorphous Fe species, which is supported by the increases in easily reducible Fe ($p < 0.05$, Table 1) and increases in Fe/Mn oxides bound ^{200}Hg ($p < 0.05$, Fig. 1a). This is because the extraction method of Fe/Mn oxides bound ^{200}Hg are the same as easily reducible Fe (i.e., $NH_2OH{\cdot}HCl$ in acetic acid), which is usually regarded as poorly crystalline or amorphous Fe (oxyhydr)oxides (Poulton and Canfield, 2005; Tessier et al., 1979). Variations in Fe species suggested the transition from well crystalline Fe (oxyhydr)oxides (e.g., goethite and hematite) to poorly crystalline Fe (oxyhydr)oxides (e.g., ferrihydrite) and then to Fe-S minerals (e.g., pyrite) in flooded paddy soil during the rice-growing period (Huang et al., 2021; Kappler et al., 2021). The studies have reported that poorly crystalline or amorphous Fe species are more active in co-precipitation or adsorption of free ^{200}Hg released from the organic matter due to the larger specific surface area

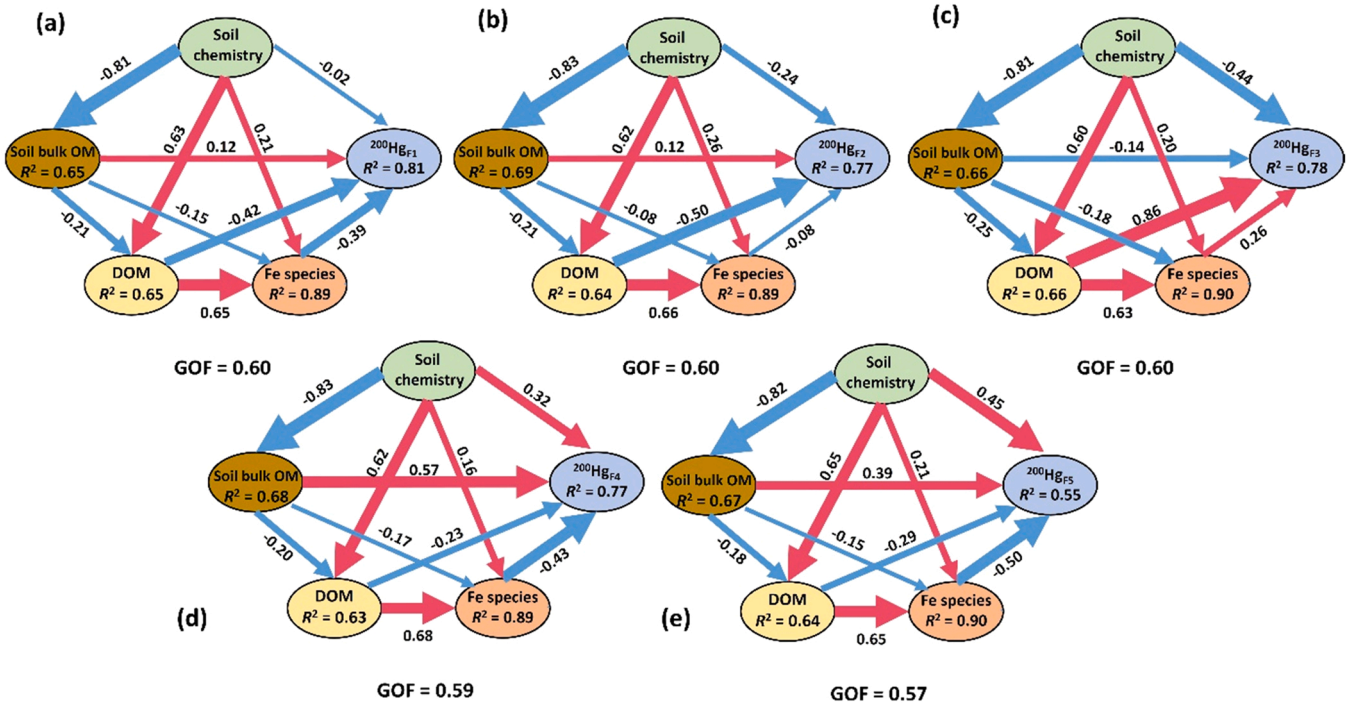

Fig. 4. Partial least squares path modeling (PLS-PM) showing the cascade relationships among soil chemistry, soil bulk organic matter, dissolved organic matter, iron species and the concentration of newly introduced Hg in different fractions in paddy soils. (a) Soluble and exchangeable ^{200}Hg; (b) carbonates bound ^{200}Hg; (c) Fe/Mn oxides bound ^{200}Hg; (d) organic matter bound ^{200}Hg; (e) residual ^{200}Hg. Red and blue arrows represent positive and negative flows of causality, respectively. The numbers on the arrows show standardized path coefficients. R^2 represents the variance of the dependent variable explained by the model. GOF represents goodness of fit.

and higher reactivity than well crystalline Fe (oxyhydr)oxides (Bao et al., 2021; Tiffreau et al., 1995). Furthermore, poorly crystalline or amorphous Fe (oxyhydr)oxides were found as a sink of DOM (Lv et al., 2016), and DOM, in return, could stabilize Fe (oxyhydr)oxides (Aiken et al., 2011). As a result, the formation of an Fe-OM (colloidal) system may coagulate Hg and affect the behaviors of the newly deposited Hg (Bao et al., 2021). However, more studies are needed to uncover the role of the Fe-OM system (Chen et al., 2020; Wang et al., 2017; Zeng et al., 2020) on the mobility and bioavailability of Hg in redox fluctuating environments. Significantly, although the total Mn concentration is lower than that of TFe, more studies are needed to study the role of Mn oxides on the fate of Hg, especially the immobilization of heavy metals by reduced sulfur coupled Mn oxides (Sun et al., 2020). Moreover, the interactions between Mn and DOM were also reported (Li et al., 2021).

It is noted that the pool of residual ^{200}Hg decreased in the redistribution of the newly deposited Hg during the rice-growing period. One possible explanation is that dissolution of the newly formed HgS (i.e., residual Hg) occurs in flooded soils. A study by Li et al. (2022) found that the dissolution of α-HgS increased the bioavailable Hg in methylation. In addition, the potential dissolution of bulk HgS induced by the formation of Hg-(poly)sulfide complexes was suggested in some periodically flooded soils (e.g., water-level fluctuation areas of reservoirs, Liu et al., 2018) and peatlands (Wang et al., 2021). However, the formation constants and measurement techniques for Hg-(poly)sulfides are still problematic.

4.3. Geochemical factors' control on partitioning and redistribution of "new" Hg in paddy soil

To unravel the controlling factors for the partitioning and redistribution of the newly deposited Hg in paddy soil, multiple analyses were applied. The correlation analysis coupled with linear regression was used to show the covariation of "new" Hg with different geochemical characteristics. Partial least squares path modeling was used to show causal relationships of the distribution pattern for the newly introduced Hg caused by various geochemical factors.

Through the correlation analysis, the significant correlations between all the isotope-enriched ^{200}Hg fractions and DOM, a(355), BIX, HIX, Fe_{carb}, Fe_{ox1}, and Fe_{ox2} (Table 2), suggesting influences of organic matter and Fe (oxyhydr)oxides on partitioning and redistribution of the newly deposited Hg. Specifically, correlations between Fe/Mn oxides bound to ^{200}Hg and soil humic acid, DOM, protein-like fluorescence compounds (peak B), and BIX (Table 2 and Fig. 3), suggested that Fe (oxyhydr)oxides are intimately linked with autochthonous OM (i.e., microbial sources) to control the partitioning and redistribution of "new" Hg in paddy soil. Similarly, opposite Spearman's r values (Spearman's $r < 0$, $p < 0.05$) were identified between those factors and OM bound ^{200}Hg (Table 2). Together with the variations of ^{200}Hg described above (i.e., the transition from organic matter bound ^{200}Hg to Fe/Mn oxides bound ^{200}Hg, Fig. 1a) and correlations here, we suggested that ^{200}Hg released from stable organic matter was recaptured by poorly crystalline Fe (oxyhydr)oxide-DOM associations during the rice-growing period and formed Hg-Fe-DOM ternary complexes. Similar ternary complexes were reported comprising different pollutants, such as As (Aftabtalab et al., 2022), Cd (Du et al., 2018), and Cr (Liao et al., 2020; Xia et al., 2020). Microbial-mediated mineralization of the recalcitrant organic matter may be the major reason for the losses of organic matter bound to ^{200}Hg because lower binding capacity and strength for Hg was found in less humified organic matter than in recalcitrant organic matter (Wang et al., 2022).

For liable Hg pools (i.e., soluble and exchangeable Hg and carbonates bound Hg), Fe (oxyhydr)oxides and organic matter are potential sinks and responsible for the aging/inactivation of "new" Hg due to their significant negative correlations (soluble and exchangeable ^{200}Hg versus humic acid, DOM, Fe_{carb} and Feo_{x1}; carbonates bound ^{200}Hg versus DOM, Fe_{carb} and Fe_{ox1}) (Table 2 and Fig. 3). Moreover, the negative covariations of soluble and exchangeable ^{200}Hg and carbonates bound ^{200}Hg with BIX indicate that increases in autochthonous DOM may

decrease the liable Hg pools, which further suggests that rhizosphere reactions and microbial metabolism could decrease the liable Hg pools. This finding is different from the traditional understanding that the formation of low molecular weight OM (e.g., low molecular weight organic acids) promotes the release of Hg to aqueous phases (Yin et al., 2018). Associations of Fe (oxyhydr)oxides-DOM are likely the reason (Bao et al., 2021).

The ternary system, Fe (oxyhydr)oxide-OM-newly deposited Hg, highlighted above was also evidenced by PLS-PM (Fig. 4). Specifically, considerable effect from DOM for Fe/Mn oxides bound ^{200}Hg, suggesting that Fe-OM interactions promote the distribution of "new" Fe(oxyhydr)oxides. In contrast, contributions from Fe species to organic matter bound ^{200}Hg implied competitive binding of ^{200}Hg between bulk SOM and Fe (oxyhydr)oxides during the rice-growing period. Typically, Fe (oxyhydr)oxides and OM often interact with each other in natural environments due to the strong binding ability between –COOH/phenolic –OH groups on OM and –OH groups on Fe (oxyhydr)oxides (Bao et al., 2021; Kleber et al., 2015). Two binding mechanisms of the newly deposited Hg by the Fe (oxyhydr)oxide-OM system were suggested: (1) ^{200}Hg act as a "bridge" connecting Fe (oxyhydr)oxides and OM to form Fe-^{200}Hg-OM associations, and (2) ^{200}Hg bind with OM associated with Fe (oxyhydr)oxides to form ^{200}Hg-OM-Fe associations (Bao et al., 2021).

The previous studies have reported that Fe-OM interactions showed significant influences on the fate of other heavy metals/metalloids (e.g., Cr, U, and As) (Al-Sid-Cheikh et al., 2015; Bao et al., 2021; Huang et al., 2021; Liao et al., 2020). This work further demonstrates that interactions between Fe(oxyhydr)oxides and DOM dominate the distribution of the newly deposited Hg in paddy soil.

4.4. Implication and prospects

The geochemical fractionation (i.e., partitioning and redistribution) of the newly deposited heavy metals into terrestrial systems determine their bioavailability and bioaccessibility, further determining the environmental risks for human exposure. The previous studies have reported that the newly introduced Cd in paddy soil rapidly aged from soluble Cd to residual Cd within 56 days through an in-lab incubation experiment, suggesting a significant aging process of Cd in paddy soil (Dong et al., 2021a, 2021b). However, similar aging processes of the newly deposited Hg in paddy soil were absent in this in situ plot experiment with a longer incubation time (i.e., 110 days). This finding partially explains why lower THg but higher MeHg was observed in the artisanal Hg mining site (i.e., contaminated by atmospheric deposited Hg) in previous studies (Meng et al., 2010, 2011; Zhao et al., 2016a). In particular, a significant correlation was observed between organic matter bound ^{200}Hg and Me^{200}Hg in this study (Spearman's $r = 0.57$, $p < 0.05$, from the day 30 to day 110). Similarly, high methylation rates of DOM-bound Hg in paddy soil were found in our previous work (Liu et al., 2022). The largest pool (i.e., organic matter bound Hg) of the newly deposited Hg in paddy soil may become a potential Hg substrate fueling methylation. Therefore, other Hg pools (e.g., organic matter bound Hg) instead of merely soluble and exchangeable Hg should be considered in evaluating the environmental risks of Hg deposited from the atmosphere. Moreover, this study provides a clue to environmental implications that highlight the role of the Fe-OM association in controlling the redistribution of "new" Hg in paddy soil. The releases and further redistribution of Hg in Fe (oxyhydr)oxide-DOM-Hg associations are likely to occur when the redox condition changes. For example, the degradation of OM or reductive dissolution of Fe(III) likely releases Hg (Bravo et al., 2018).

On the other hand, we should note that the study was conducted during one rice-growing period (110 days), and the geochemical fractionation or potential aging process of deposited Hg over a longer time scale remains unclear. Therefore, a long-term study of the dynamics of "new" Hg in wetland ecosystems is needed to better evaluate the environmental risks of Hg from atmospheric deposition, such as the Mercury Experiment to Assess Atmospheric Loading in Canada and the United States (METAALICUS) project (Blanchfield et al., 2021; Branfireun et al., 2005; Harris et al., 2007; Hintelmann et al., 2002; Oswald et al., 2014). Moreover, a more solid or direct evidence is needed to show the formation of Hg-Fe-DOM ternary systems, for example, by using nanoscale secondary ion mass spectrometry (NanoSIMS) (Al-Sid-Cheikh et al., 2015; Du et al., 2018) and scanning transmission X-ray microscopy (STXM) (Xia et al., 2020).

5. Conclusions

The isotope-enriched ^{200}Hg was applied to trace partitioning and redistribution of the newly deposited Hg in paddy soil during the rice-growing period. Soil organic matter is the largest sink of the newly deposited Hg in paddy soils, followed by residual Hg, Fe/Mn oxides bound Hg, soluble and exchangeable Hg, and carbonates bound Hg. In this study, 89.4% of Hg was rapidly distributed into the organic matter since it was deposited. During the rice-growing period, redistribution of the newly deposited Hg was identified from soluble and exchangeable Hg, carbonates bound Hg, organic matter bound Hg, and residual Hg to Fe/Mn oxides bound Hg. Geochemical fractionation of the newly deposited Hg in paddy soil is likely caused by (1) microbial-mediated mineralization of soil organic matter and (2) Fe phase changes from well crystalline Fe (oxyhydr)oxides to poorly crystalline Fe (oxyhydr)oxides and then Fe-S minerals. Correlation analyses jointly with partial least squares path modeling suggested that the coupling of autochthonous OM and poorly crystalline/amorphous Fe (oxyhydr)oxides plays a predominant role in controlling the speciation of "new" Hg in paddy soils. The decreases in the residual Hg pool from the newly deposited Hg were found in this study, suggesting the aging processes of conversion to a residue Hg from newly deposited Hg was absent in paddy soils during the rice-growing period. This study also implied that soluble and exchangeable Hg is not the only bioavailable Hg pool; other pools, for example, organic matter bound Hg, may also be methylated and should be considered.

Environmental implication

For the first trial, we successfully identified the fate of newly deposited Hg in paddy soils by using enriched stable Hg isotopes. We suggested that soluble and exchangeable Hg is not the only bioavailable Hg pool; other pools, for example, organic matter bound Hg, may also be methylated and should be considered. Our findings provide new information on the speciation and bioavailability of "new" Hg in paddy soils, which would help to improve our understanding of the biogeochemical cycling and environmental risks of newly deposited Hg, especially in sensitive ecosystems (e.g., rice paddies, wetlands, and reservoirs).

CRediT authorship contribution statement

Jiang Liu: Investigation, Data curation, Formal analysis, Writing – original draft. **Lei Zhao**: Investigation, Conceptualization, Funding acquisition; Writing – review & editing. **Kun Kong**: Investigation, Data curation. **Mahmoud A. Abdelhafiz:** Writing – review & editing. **Shanyi Tian**: Formal analysis, Writing – review & editing. **Tao Jiang**: Formal analysis, Writing – review & editing. **Bo Meng**: Project administration, Conceptualization, Supervision, Writing – review & editing. **Xinbin Feng:** Resources, Writing – review & editing.

Declaration of Competing Interest

The authors declare that they have no known competing financial interests or personal relationships that could have appeared to influence the work reported in this paper.

Acknowledgments

The authors would like to acknowledge the support of the National Natural Science Foundation of China (42163009, 41703130, 42107442), the Guizhou Provincial Natural Science Foundation (Qian-Ke-He-Ji-Chu ZK [2021]Zhong-Dian 041), the CAS "Light of West China" program, and the Opening Fund of the State Key Laboratory of Environmental Geochemistry (SKLEG2021201). We thank Qiyi Meng and Ji Chen for helps with sample collection and measurement. We thank Songbo Yao and Yuqin Wang, both from Southwest University, for important help in the analysis of natural organic matter and the establishment of PLS-PM. We would also like to thank Dr. Yong Meng for XRD analysis. Finally, we thank the editors and 11 anonymous reviewers for their constructive comments.

Appendix A. Supporting information

Supplementary data associated with this article can be found in the online version at doi:10.1016/j.jhazmat.2022.128752.

References

Aftabtalab, A., Rinklebe, J., Shaheen, S.M., Niazi, N.K., Moreno-Jiménez, E., Schaller, J., Knorr, K.H., 2022. Review on the interactions of arsenic, iron (oxy)(hydr)oxides, and dissolved organic matter in soils, sediments, and groundwater in a ternary system. Chemosphere 286. https://doi.org/10.1016/j.chemosphere.2021.131790.

Aiken, G.R., Hsu-kim, H., Ryan, J.N., 2011. Influence of dissolved organic matter on the environmental fate of metals, nanoparticles, and colloids. Environ. Sci. Technol. 3196–3201. https://doi.org/10.1021/es103992s.

Al-Sid-Cheikh, M., Pédrot, M., Dia, A., Guenet, H., Vantelon, D., Davranche, M., Gruau, G., Delhaye, T., 2015. Interactions between natural organic matter, sulfur, arsenic and iron oxides in compounds within riparian wetlands: NanoSIMS and X-ray adsorption spectroscopy evidences. Sci. Total Environ. 515–516, 118–128. https://doi.org/10.1016/j.scitotenv.2015.02.047.

Ao, M., Xu, X., Wu, Y., Zhang, C., Meng, B., Shang, L., Liang, L., Qiu, R., Wang, S., Qian, X., Zhao, L., Qiu, G., 2020. Newly deposited atmospheric mercury in a simulated rice ecosystem in an active mercury mining region: High loading, accumulation, and availability. Chemosphere 238, 124630. https://doi.org/10.1016/j.chemosphere.2019.124630.

Ariya, P.A., Amyot, M., Dastoor, A., Deeds, D., Feinberg, A., Kos, G., Poulain, A., Ryjkov, A., Semeniuk, K., Subir, M., Toyota, K., 2015. Mercury physicochemical and biogeochemical transformation in the atmosphere and at atmospheric interfaces: A review and future directions. Chem. Rev. 115, 3760–3802. https://doi.org/10.1021/cr500667e.

Aslam, M.W., Meng, B., Abdelhafiz, M.A., Liu, J., Feng, X., 2022. Unravelling the interactive effect of soil and atmospheric mercury influencing mercury distribution and accumulation in the soil-rice system. Sci. Total Environ. 803, 149967 https://doi.org/10.1016/j.scitotenv.2021.149967.

Bao, Y., Bolan, N.S., Lai, J., Wang, Y., Jin, X., Kirkham, M.B., Wu, X., Fang, Z., Zhang, Y., Wang, H., 2021. Interactions between organic matter and Fe (hydr)oxides and their influences on immobilization and remobilization of metal(loid)s: A review. Crit. Rev. Environ. Sci. Technol. https://doi.org/10.1080/10643389.2021.1974766.

Bishop, M.E., Dong, H., Glasser, P., Briggs, B.R., Pentrak, M., Stucki, J.W., 2020. Microbially mediated iron redox cycling of subsurface sediments from Hanford Site, Washington State, USA. Chem. Geol. 546, 119643 https://doi.org/10.1016/j.chemgeo.2020.119643.

Blanchfield, P.J., Rudd, J.W.M., Hrenchuk, L.E., Amyot, M., Babiarz, C.L., Beaty, K.G., Bodaly, R.A.D., Branfireun, B.A., Gilmour, C.C., Graydon, J.A., Hall, B.D., Harris, R. C., Heyes, A., Hintelmann, H., Hurley, J.P., Kelly, C.A., Krabbenhoft, D.P., Lindberg, S.E., Mason, R.P., Paterson, M.J., Podemski, C.L., Sandilands, K.A., Southworth St, G.R., Louis, V.L., Tate, L.S., Tate, M.T., 2021. Experimental evidence for recovery of mercury-contaminated fish populations. Nature 601, 74–78. https://doi.org/10.1038/s41586-021-04222-7.

Bonnissel-Gissinger, P., Alnot, M., Lickes, J.P., Ehrhardt, J.J., Behra, P., 1999. Modeling the adsorption of mercury(II) on (hydr)oxides II: α-FeOOH (goethite) and amorphous silica. J. Colloid Interface Sci. 215, 313–322. https://doi.org/10.1006/jcis.1999.6263.

Branfireun, B.A., Krabbenhoft, D.P., Hintelmann, H., Hunt, R.J., Hurley, J.P., Rudd, J.W. M., 2005. Speciation and transport of newly deposited mercury in a boreal forest wetland: A stable mercury isotope approach. Water Resour. Res. 41, 1–11. https://doi.org/10.1029/2004WR003219.

Bravo, A.G., Zopfi, J., Buck, M., Xu, J., Bertilsson, S., Schaefer, J.K., Poté, J., Cosio, C., 2018. Geobacteraceae are important members of mercury-methylating microbial communities of sediments impacted by waste water releases. ISME J. 12, 802–812. https://doi.org/10.1038/s41396-017-0007-7.

Carter, M.R., Gregorich, E.G., 2007. Soil Sampling and Methods of Analysis. CRC Press, Boca Raton, FL.

Chen, C., Hall, S.J., Thompson, A., 2020. Iron-mediated organic matter decomposition in humid soils can counteract protection. Nat. Commun. 11, 2255. https://doi.org/10.1038/s41467-020-16071-5.

Claff, S.R., Sullivan, L.A., Burton, E.D., Bush, R.T., 2010. A sequential extraction procedure for acid sulfate soils: Partitioning of iron. Geoderma 155, 224–230. https://doi.org/10.1016/j.geoderma.2009.12.002.

Dong, Q., Liu, Y., Liu, G., Guo, Y., Yang, Q., Shi, J., Hu, L., Liang, Y., Yin, Y., Cai, Y., Jiang, G., 2021a. Aging and phytoavailability of newly introduced and legacy cadmium in paddy soil and their bioaccessibility in rice grain distinguished by enriched isotope tracing. J. Hazard. Mater. 417, 125998 https://doi.org/10.1016/j.jhazmat.2021.125998.

Dong, Q., Liu, Y., Liu, G., Guo, Y., Yang, Q., Shi, J., Hu, L., Liang, Y., Yin, Y., Cai, Y., Jiang, G., 2021b. Enriched isotope tracing to reveal the fractionation and lability of legacy and newly introduced cadmium under different amendments. J. Hazard. Mater. 403, 123975 https://doi.org/10.1016/j.jhazmat.2020.123975.

Du, H., Peacock, C.L., Chen, W., Huang, Q., 2018. Binding of Cd by ferrihydrite organo-mineral composites: Implications for Cd mobility and fate in natural and contaminated environments. Chemosphere 207, 404–412. https://doi.org/10.1016/j.chemosphere.2018.05.092.

Du, L., Zhu, Z., Qi, Y., Zou, D., Zhang, G., Zeng, X., Ge, T., Wu, J., Xiao, Z., 2020. Effects of different stoichiometric ratios on mineralisation of root exudates and its priming effect in paddy soil. Sci. Total Environ. 743, 140808 https://doi.org/10.1016/j.scitotenv.2020.140808.

Feng, X., Li, P., Qiu, G., Wang, S., Li, G., Shang, L., Meng, B., Jiang, H., Bai, W., Li, Z., Fu, X., 2008. Human exposure to methylmercury through rice intake in mercury mining areas, Guizhou Province, China. Environ. Sci. Technol. 42, 326–332. https://doi.org/10.1021/es071948x.

Feyte, S., Tessier, A., Gobeil, C., Cossa, D., 2010. In situ adsorption of mercury, methylmercury and other elements by iron oxyhydroxides and organic matter in lake sediments. Appl. Geochem. 25, 984–995. https://doi.org/10.1016/j.apgeochem.2010.04.005.

Fu, X.W., Feng, X., Shang, L.H., Wang, S.F., Zhang, H., 2012. Two years of measurements of atmospheric total gaseous mercury (TGM) at a remote site in Mt. Changbai area, Northeastern China. Atmos. Chem. Phys. 12, 4215–4226. https://doi.org/10.5194/acp-12-4215-2012.

Fu, X.W., Zhang, H., Yu, B., Wang, X., Lin, C.J., Feng, X.B., 2015. Observations of atmospheric mercury in China: A critical review. Atmos. Chem. Phys. 15, 9455–9476. https://doi.org/10.5194/acp-15-9455-2015.

Gerbig, C.A., Kim, C.S., Stegemeier, J.P., Ryan, J.N., Aiken, G.R., 2011. Formation of nanocolloidal metacinnabar in mercury-DOM-sulfide systems. Environ. Sci. Technol. 45, 9180–9187. https://doi.org/10.1021/es201837h.

Gilmour, C.C., Riedel, G.S., Ederington, M.C., Bell, J.T., Benoit, J.M., Gill, G.A., Stordal, M.C., 1998. Methylmercury concentrations and production rates across a trophic gradient in the Northern Everglades. Biogeochemistry 40, 327–345. https://doi.org/10.1023/A:1005972708616.

Graham, A.M., Aiken, G.R., Gilmour, C.C., 2012. Dissolved organic matter enhances microbial mercury methylation under sulfidic conditions. Environ. Sci. Technol. 46, 2715–2723. https://doi.org/10.1021/es203658f.

Harris, R.C., Rudd, J.W.M., Amyot, M., Babiarz, C.L., Beaty, K.G., Blanchfield, P.J., Bodaly, R.A., Branfireun, B.A., Gilmour, C.C., Graydon, J.A., Heyes, A., Hintelmann, H., Hurley, J.P., Kelly, C.A., Krabbenhoft, D.P., Lindberg, S.E., Mason, R.P., Paterson, M.J., Podemski, C.L., Robinson, A., Sandilands, K.A., Southworth St., G.R., Louis, V., Tate, M.T., 2007. Whole-ecosystem study shows rapid fish-mercury response to changes in mercury deposition. Proc. Nati. Acad. Sci. U.S.A. 104, 16586–16591. https://doi.org/10.1073/pnas.0704186104.

Hintelmann, H., Harris, R., Heyes, A., Hurley, J.P., Kelly, C.A., Krabbenhoft, D.P., Lindberg, S., Rudd, J.W.M., Scott, K.J., St. Louis, V., 2002. Reactivity and mobility of new and old mercury deposition in a boreal forest ecosystem during the first year of the METAALICUS study. Environ. Sci. Technol. 36, 5034–5040. https://doi.org/10.1021/es025572t.

Hsu-kim, H., Kucharzyk, K.H., Zhang, T., Deshusses, M.A., 2013. Mechanisms regulating mercury bioavailability for methylating microorganisms in the aquatic environment: a critical review. Environ. Sci. Technol. 47, 2441–2456. https://doi.org/10.1021/es304370g.

Huang, J., Jones, A., Waite, T.D., Chen, Y., Huang, X., Rosso, K.M., Kappler, A., Mansor, M., Tratnyek, P.G., Zhang, H., 2021. Fe(II) redox chemistry in the environment. Chem. Rev. 121, 8161–8233. https://doi.org/10.1021/acs.chemrev.0c01286.

Jiang, T., Kaal, J., Liang, J., Zhang, Y., Wei, S., Wang, D., Green, N.W., 2017. Composition of dissolved organic matter (DOM) from periodically submerged soils in the Three Gorges Reservoir areas as determined by elemental and optical analysis, infrared spectroscopy, pyrolysis-GC-MS and thermally assisted hydrolysis and methylation. Sci. Total Environ. 603–604, 461–471. https://doi.org/10.1016/j.scitotenv.2017.06.114.

Jonsson, S., Skyllberg, U., Nilsson, M.B., Lundberg, E., Andersson, A., Björn, E., 2014. Differentiated availability of geochemical mercury pools controls methylmercury levels in estuarine sediment and biota. Nat. Commun. 5, 4624. https://doi.org/10.1038/ncomms5624.

Kappler, A., Bryce, C., Mansor, M., Lueder, U., Byrne, J.M., Swanner, E.D., 2021. An evolving view on biogeochemical cycling of iron. Nat. Rev. Microbiol. 19, 360–374. https://doi.org/10.1038/s41579-020-00502-7.

Kleber, M., Eusterhues, K., Keiluweit, M., Mikutta, C., Mikutta, R., Nico, P.S., 2015. Mineral-organic associations: Formation, properties, and relevance in soil environments. Adv. Agron. 130, 1–140. https://doi.org/10.1016/bs.agron.2014.10.005.

Kögel-Knabner, I., Amelung, W., Cao, Z., Fiedler, S., Frenzel, P., Jahn, R., Kalbitz, K., Kölbl, A., Schloter, M., 2010. Biogeochemistry of paddy soils. Geoderma 157, 1–14. https://doi.org/10.1016/j.geoderma.2010.03.009.

Lalonde, K., Mucci, A., Ouellet, A., Gélinas, Y., 2012. Preservation of organic matter in sediments promoted by iron. Nature 483, 198–200. https://doi.org/10.1038/nature10855.

Liao, P., Pan, C., Ding, W., Li, W., Yuan, S., Fortner, J.D., Giammar, D.E., 2020. Formation and transport of Cr(III)-NOM-Fe colloids upon reaction of Cr(VI) with NOM-Fe(II) colloids at anoxic − oxic interfaces. Environ. Sci. Technol. 54, 4256–4266. https://doi.org/10.1021/acs.est.9b07934.

Liu, J., Jiang, T., Wang, F., Zhang, J., Wang, D., Huang, R., Yin, D., Liu, Z., Wang, J., 2018. Inorganic sulfur and mercury speciation in the water level fluctuation zone of the Three Gorges Reservoir, China: the role of inorganic reduced sulfur on mercury methylation. Environ. Pollut. 237, 1112–1123. https://doi.org/10.1016/j.envpol.2017.11.045.

Liu, J., Liang, J., Bravo, A.G., Wei, S., Yang, C., Wang, D., Jiang, T., 2021b. Anaerobic and aerobic biodegradation of soil-extracted dissolved organic matter from the water-level-fluctuation zone of the Three Gorges Reservoir region, China. Sci. Total Environ. 764, 142857 https://doi.org/10.1016/j.scitotenv.2020.142857.

Liu, J., Lu, B., Poulain, A.J., Zhang, R., Zhang, T., Feng, X., Meng, B., 2022. The underappreciated role of natural organic matter bond Hg(II) and nanoparticulate HgS as substrates for methylation in paddy soils across a Hg concentration gradient. Environ. Pollut., 112075 https://doi.org/10.1016/j.envpol.2021.118321.

Liu, C., Massey, M.S., Latta, D.E., Xia, Y., Li, F., Gao, T., Hua, J., 2021c. Fe(II)-induced transformation of iron minerals in soil ferromanganese nodules. Chem. Geol. 559, 119901 https://doi.org/10.1016/j.chemgeo.2020.119901.

Liu, J., Meng, B., Poulain, A.J., Meng, Q., Feng, X., 2021a. Stable isotope tracers identify sources and transformations of mercury in rice (*Oryza sativa L.*) growing in a mercury mining area. Fundam. Res. 1, 259–268. https://doi.org/10.1016/j.fmre.2021.04.003.

Li, H., Li, Y., Tang, W., Liu, Y., Zheng, L., Xu, N., Li, Y.-F., Xu, D., Gao, Y., Zhao, J., 2022. Bioavailability and methylation of bulk mercury sulfide in paddy soils: New insights into mercury risks in rice paddies. J. Hazard. Mater. 424, 127394 https://doi.org/10.1016/j.jhazmat.2021.127394.

Li, H., Santos, F., Butler, K., Herndon, E., 2021. A critical review on the multiple roles of manganese in stabilizing and destabilizing soil organic matter. Environ. Sci. Technol. 55, 12136–12152. https://doi.org/10.1021/acs.est.1c00299.

Li, Y., Wang, Y., Zhang, Q., Hu, W., Zhao, J., Chen, Y., Zhong, H., Wang, G., Zhang, Z., Gao, Y., 2019. Elemental sulfur amendment enhance methylmercury accumulation in rice (*Oryza sativa* L.) grown in Hg mining polluted soil. J. Hazard. Mater. 379, 120701 https://doi.org/10.1016/j.jhazmat.2019.05.094.

Lucotte, M., Schetagne, R., Therien, N., Langlois, C., Tremblay, A., 1999. Mercury in the Biogeochemical Cycle: Natural Environments and Hydroelectric Reservoirs of Northern Québec (Canada). Springer, Berlin.

Lu, B.Q., Liu, J., Lv, W.Q., Li, S., Feng, X.B., Meng, B., 2021. Distribution characteristics of mercury occurrences in the paddy soil of Hg mining area and its effect on mercury methylation. Bull. Miner. Petrol. Geochem. 40, 1–9 (In Chinese with English abstract).

Lv, J., Zhang, S., Wang, S., Luo, L., Cao, D., Christie, P., 2016. Molecular-scale investigation with ESI-FT-ICR-MS on fractionation of dissolved organic matter induced by adsorption on iron oxyhydroxides. Environ. Sci. Technol. 50, 2328–2336. https://doi.org/10.1021/acs.est.5b04996.

Manceau, A., Wang, J., Rovezzi, M., Glatzel, P., Feng, X., 2018. Biogenesis of mercury-sulfur nanoparticles in plant leaves from atmospheric gaseous mercury. Environ. Sci. Technol. 52, 3935–3948. https://doi.org/10.1021/acs.est.7b05452.

Meng, B., Feng, X., Qiu, G., Cai, Y., Wang, D., Li, P., Shang, L., Sommar, J., 2010. Distribution patterns of inorganic mercury and methylmercury in tissues of rice (*Oryza sativa* L.) plants and possible bioaccumulation pathways. J. Agric. Food Chem. 58, 4951–4958. https://doi.org/10.1021/jf904557x.

Meng, B., Feng, X., Qiu, G., Liang, P., Li, P., Chen, C., Shang, L., 2011. The process of methylmercury accumulation in rice (*Oryza sativa* L.). Environ. Sci. Technol. 45, 2711–2717. https://doi.org/10.1021/es103384v.

Meng, B., Li, Y., Cui, W., Jiang, P., Liu, G., Wang, Y., Richards, J., Feng, X., Cai, Y., 2018. Tracing the uptake, transport, and fate of mercury in Sawgrass (*Cladium jamaicense*) in the Florida Everglades using a multi-isotope technique. Environ. Sci. Technol. 52, 3384–3391. https://doi.org/10.1021/acs.est.7b04150.

Murphy, K.R., Butler, K.D., Spencer, R.G.M., Stedmon, C.A., Boehme, J.R., Aiken, G.R., 2010. Measurement of dissolved organic matter fluorescence in aquatic environments: an interlaboratory comparison. Environ. Sci. Technol. 44, 9405–9412. https://doi.org/10.1021/es102362t.

Mu, C., Schuster, P.F., Abbott, B.W., Kang, S., Guo, J., Sun, S., Wu, Q., Zhang, T., 2020. Permafrost degradation enhances the risk of mercury release on Qinghai-Tibetan Plateau. Sci. Total Environ. 708, 135127 https://doi.org/10.1016/j.scitotenv.2019.135127.

O'Connor, D., Hou, D., Ok, Y.S., Mulder, J., Duan, L., Wu, Q., Wang, S., Tack, F.M.G., Rinklebe, J., 2019. Mercury speciation, transformation, and transportation in soils, atmospheric flux, and implications for risk management: A critical review. Environ. Int. 126, 747–761. https://doi.org/10.1016/j.envint.2019.03.019.

Orihel, D.M., Paterson, M.J., Blanchfield, P.J., Bodaly, R.A.D., Gilmour, C.C., Hintelmann, H., 2008. Temporal changes in the distribution, methylation, and bioaccumulation of newly deposited mercury in an aquatic ecosystem. Environ. Pollut. 154, 77–88. https://doi.org/10.1016/j.envpol.2007.12.030.

Oswald, C.J., Heyes, A., Branfireun, B.A., 2014. Fate and transport of ambient mercury and applied mercury isotope in terrestrial upland soils: Insights from the METAALICUS watershed. Environ. Sci. Technol. 48, 1023–1031. https://doi.org/10.1021/es404260f.

Paterson, M.J., Blanchfield, P.J., Podemski, C., Holger, H., Gilmour, C.C., Harris, R., Ogrinc, N., Rudd, J.W.M., Sandilands, K.A., 2006. Bioaccumulation of newly deposited mercury by fish and invertebrates: an enclosure study using stable mercury isotopes. Can. J. Fish. Aquat. Sci. 63, 2213–2224. https://doi.org/10.1139/f06-118.

Poulton, S.W., Canfield, D.E., 2005. Development of a sequential extraction procedure for iron: implications for iron partitioning in continentally derived particulates. Chem. Geol. 214, 209–221. https://doi.org/10.1016/j.chemgeo.2004.09.003.

Qiu, G.L., Feng, X.B., Li, P., Wang, S.F., Li, G.H., Shang, L.H., Fu, X.W., 2008. Methylmercury accumulation in rice (*Oryza sativa* L.) grown at abandoned mercury mines in Guizhou, China. J. Agric. Food Chem. 56, 2465–2468. https://doi.org/10.1021/jf073391a.

Ratié, G., Vantelon, D., Lot, E., Bihannic, I., Pierson-wickmann, A.C., Davranche, M., 2019. Iron speciation at the riverbank surface in wetland and potential impact on the mobility of trace metals. Sci. Total Environ. 651, 443–455. https://doi.org/10.1016/j.scitotenv.2018.09.143.

Riedel, T., Zak, D., Biester, H., Dittmar, T., 2013. Iron traps terrestrially derived dissolved organic matter at redox interfaces. Proc. Natl. Acad. Sci. U.S.A. 110, 10101–10105. https://doi.org/10.1073/pnas.1221487110.

Rolfhus, K.R., Hurley, J.P., Bodaly, R.A., Perrine, G., 2015. Production and retention of methylmercury in inundated boreal forest soils. Environ. Sci. Technol. 49, 3482–3489. https://doi.org/10.1021/es505398z.

Schroeder, W.H., Anlauf, K.G., Barrie, L.A., Lu, J.Y., Steffen, A., Schneeberger, D.R., Berg, T., 1998. Arctic springtime depletion of mercury. Nature 394, 331–332. https://doi.org/10.1038/28530.

Skyllberg, U., 2008. Competition among thiols and inorganic sulfides and polysulfides for Hg and MeHg in wetland soils and sediments under suboxic conditions: illumination of controversies and implications for MeHg net production. J. Geophys. Res.: Biogeosci. 113. https://doi.org/10.1029/2008JG000745.

Skyllberg, U., Bloom, P.R., Qian, J., Lin, C.M., Bleam, W.F., 2006. Complexation of mercury (II) in soil organic matter: EXAFS evidence for linear two-coordination with reduced sulfur groups. Environ. Sci. Technol. 40 (13), 4174–4180. https://doi.org/10.1021/es0600577.

Skyllberg, U., Persson, A., Tjerngren, I., Kronberg, R., Drott, A., Meili, M., Björn, E., 2021. Chemical speciation of mercury, sulfur and iron in a dystrophic boreal lake sediment, as controlled by the formation of mackinawite and framboidal pyrite. Geochim. Cosmochim. Acta 294, 106–125. https://doi.org/10.1016/j.gca.2020.11.022.

Slotznick, S.P., Sperling, E.A., Tosca, N.J., Miller, A.J., Clayton, K.E., van Helmond, N.A. G.M., Slomp, C.P., Swanson-Hysell, N.L., 2020. Unraveling the Mineralogical Complexity of Sediment Iron Speciation Using Sequential Extractions. e2019GC008666 Geochem. Geophys. Geosyst. 21. https://doi.org/10.1029/2019GC008666.

Sun, Q., Cui, P., Wu, S., Liu, C., Fan, T., Alves, M.E., Cheng, H., Huang, M., Zhou, D., Wang, Y., 2020. Role of reduced sulfur in the transformation of Cd(II) immobilized by δ-MnO_2. Environ. Sci. Technol. 54, 14955–14963. https://doi.org/10.1021/acs.est.0c02936.

Sörbo, B., 1987. Sulfate: turbidmetric and nephelometric methods. Method. Enzymol. 143, 3–6. https://doi.org/10.1016/0076-6879(87)43003-6.

Tessier, A., Campbell, P.G.C., Bisson, M., 1979. Sequential extraction procedure for the speciation of particulate trace metals. Anal. Chem. 51, 844–851 https://0003-2700/79/0351-0844$01.00/0.

Tiffreau, C., Lützenkirchen, J., Behra, P., 1995. Modeling the adsorption of mercury(II) on (Hydr)oxides: I. Amorphous iron oxide and α-quartz. J. Colloid Interface Sci. 172, 82–93. https://doi.org/10.1006/jcis.1995.1228.

Viollier, E., Inglett, P.W., Hunter, K., Roychoudhury, A.N., Cappellen, P.V., 2000. The ferrozine method revisited: Fe(II)/Fe(III) determination in natural waters. Appl. Geochem. 15, 785–790. https://doi.org/10.1016/S0883-2927(99)00097-9.

Wang, J., Feng, X., Anderson, C.W.N., Qiu, G., Ping, L., Bao, Z., 2011. Ammonium thiosulphate enhanced phytoextraction from mercury contaminated soil – Results from a greenhouse study. J. Hazard. Mater. 186, 119–127. https://doi.org/10.1016/j.jhazmat.2010.10.097.

Wang, Y., Liu, J., Liem-Nguyen, V., Tian, S., Zhang, S., Wang, D., Jiang, T., 2022. Binding strength of mercury (II) to different dissolved organic matter: the roles of DOM properties and sources. Sci. Total Environ. 807, 150979 https://doi.org/10.1016/j.scitotenv.2021.150979.

Wang, Y., Wang, H., He, J., Feng, X., 2017. Iron-mediated soil carbon response to water-table decline in an alpine wetland. Nat. Commun. 8, 1–9. https://doi.org/10.1038/ncomms15972.

Wang, B., Zhong, S., Bishop, K., Nilsson, M.B., Hu, H., Eklöf, K., Bravo, A.G., Åkerblom, S., Bertilsson, S., Björn, E., Skyllberg, U., 2021. Biogeochemical influences on net methylmercury formation proxies along a peatland chronosequence. Geochim. Cosmochim. Acta 308, 188–203. https://doi.org/10.1016/j.gca.2021.06.010.

Wilson, H.F., Xenopoulos, M.A., 2009. Effects of agricultural land use on the composition of fluvial dissolved organic matter. Nat. Geosci. 2, 37–41. https://doi.org/10.1038/ngeo391.

Xia, X., Yang, J., Yan, Y., Wang, J., Hu, Y., Zeng, X., 2020. Molecular sorption mechanisms of Cr(III) to organo-ferrihydrite coprecipitates using synchrotron-based EXAFS and STXM techniques. Environ. Sci. Technol. 54, 12989–12997. https://doi.org/10.1021/acs.est.0c02872.

Xu, Y., He, T., Wu, P., Yin, D., Shu, R., 2021. Fulvic acid: a key factor governing mercury bioavailability in a polluted plateau wetland. Water Res. 205, 117652 https://doi.org/10.1016/j.watres.2021.117652.

Yin, R., Gu, C., Feng, X., Hurley, J.P., Krabbenhoft, D.P., Lepak, R.F., Zhu, W., Zheng, L., Hu, T., 2016. Distribution and geochemical speciation of soil mercury in Wanshan

Hg mine: effects of cultivation. Geoderma 272, 32–38. https://doi.org/10.1016/j.geoderma.2016.03.003.
Yin, D., Wang, Y., Jiang, T., Qin, C., Xiang, Y., Chen, Q., Xue, J., Wang, D., 2018. Methylmercury production in soil in the water-level-fluctuating zone of the Three Gorges Reservoir, China: the key role of low-molecular-weight organic acids. Environ. Pollut. 235, 186–196. https://doi.org/10.1016/j.envpol.2017.12.072.
Zeng, Q., Huang, L., Ma, J., Zhu, Z., He, C., Shi, Q., Liu, W., Wang, X., Xia, Q., Dong, H., 2020. Bio-reduction of ferrihydrite-montmorillonite-organic matter complexes: Effect of montmorillonite and fate of organic matter. Geochim. Cosmochim. Acta 276, 327–344. https://doi.org/10.1016/j.gca.2020.03.011.
Zhang, H., Feng, X.B., Larssen, T., Qiu, G.L., Vogt, R.D., 2010. In inland China, rice, rather than fish, is the major pathway for methylmercury exposure. Environ. Health Perspect. 118, 1183–1188. https://doi.org/10.1289/ehp.1001915.
Zhang, L., Wu, S., Zhao, L., Lu, X., Pierce, E.M., Gu, B., 2019. Mercury sorption and desorption on organo-mineral particulates as a source for microbial methylation. Environ. Sci. Technol. 53, 2426–2433. https://doi.org/10.1021/acs.est.8b06020.
Zhao, L., 2016. Distribution patterns and methylation/demethylation rate of mercury in rice paddy in Hg mining area (ph. D. thesis). Southwest University (In Chinese with English abstract).
Zhao, L., Anderson, C.W.N., Qiu, G., Meng, B., Wang, D., Feng, X., 2016a. Mercury methylation in paddy soil: source and distribution of mercury species at a Hg mining area, Guizhou Province, China. Biogeosciences 13, 2429–2440. https://doi.org/10.5194/bg-13-2429-2016.
Zhao, L., Meng, B., Feng, X., 2020. Mercury methylation in rice paddy and accumulation in rice plant: a review. Ecotoxicol. Environ. Saf. 195, 110462 https://doi.org/10.1016/j.ecoenv.2020.110462.
Zhao, L., Qiu, G., Anderson, C.W.N., Meng, B., Wang, D., Shang, L., Yan, H., Feng, X., 2016b. Mercury methylation in rice paddies and its possible controlling factors in the Hg mining area, Guizhou Province, southwest China. Environ. Pollut. 215, 1–9. https://doi.org/10.1016/j.envpol.2016.05.001.
Zhu, Y., Ma, L.Q., Gao, B., Bonzongo, J.C., Harris, W., Gu, B., 2012. Transport and interactions of kaolinite and mercury in saturated sand media. J. Hazard. Mater. 213–214, 93–99. https://doi.org/10.1016/j.jhazmat.2012.01.061.